Single-Atom Mn Active Site in a Triol-Stabilized β-Anderson Manganohexamolybdate for Enhanced Catalytic Activity towards Adipic Acid Production

Jianhui Luo [1,2,†], **Yichao Huang** [3,†], **Bin Ding** [1,2], **Pingmei Wang** [1,2], **Xiangfei Geng** [1,2], **Jiangwei Zhang** [3,*] and **Yongge Wei** [3,*]

[1] Research Institute of Petroleum Exploration & Development (RIPED), Petro China, Beijing 100083, China; luojh@petrochina.com.cn (J.L.); dingb@petrochina.com.cn (B.D.); wangpm@petrochina.com.cn (P.W.); gengxf@petrochina.com.cn (X.G.)
[2] Key Laboratory of Nano Chemistry (KLNC), CNPC, Beijing 100083, China
[3] Key Lab of Organic Optoelectronics & Molecular Engineering of Ministry of Education, Department of Chemistry, Tsinghua University, Beijing 100084, China; yichaoh@126.com
* Correspondence: jwzhang@dicp.ac.cn (J.Z.); yonggewei@mail.tsinghua.edu.cn (Y.W.); Tel.: +86-010-627-97852 (J.Z. & Y.W)
† These authors contributed equally to this work.

Abstract: Adipic acid is an important raw chemical for the commercial production of polyamides and polyesters. The traditional industrial adipic acid production utilizes nitric acid to oxidize KA oil (mixtures of cyclohexanone and cyclohexanol), leading to the emission of N_2O and thus causing ozone depletion, global warming, and acid rain. Herein, we reported an organically functionalized β-isomer of Anderson polyoxometalates (POMs) nanocluster with single-atom Mn, $\beta\text{-}\{[H_3NC(CH_2O)_3]_2MnMo_6O_{18}\}^-$ (**1**), as a highly active catalyst to selectively catalyze the oxidation of cyclohexanone, cyclohexanol, or KA oil with atom economy use of 30% H_2O_2 for the eco-friendly synthesis of adipic acid. The catalyst has been characterized by single crystal and powder XRD, XPS, ESI-MS, FT-IR, and NMR. A cyclohexanone (cyclohexanol) conversion of >99.9% with an adipic acid selectivity of ~97.1% (~85.3%) could be achieved over catalyst **1** with high turnover frequency of 2427.5 h^{-1} (2132.5 h^{-1}). It has been demonstrated that the existence of Mn^{3+} atom active site in catalyst **1** and the special butterfly-shaped topology of POMs both play vital roles in the enhancement of catalytic activity.

Keywords: polyoxometalates; catalytic oxidation; single-atom; active site engineering; KA oil; adipic acid

1. Introduction

Adipic acid (AA) is one of the most important industrial chemicals for the production of polyamides, polyesters, and polyurethane resins [1,2]. Additionally, AA is widely used as an approved additive in cosmetics, gelatins, lubricants, fertilizers, adhesives, insecticides, paper, and waxes [3]. The global AA production is more than 3.5 million of metric tons with a rapid demand growth of 4–5% annually [4]. However, in traditional industrial production, AA is mainly generated by the oxidization of KA oil (i.e., a mixture of cyclohexanol and cyclohexanone) with an excess of 50–60% nitric acid at 60–80 °C catalyzed with copper(II) and ammonium metavanadate. This process will suffer from the corrosion of reaction vessels and inevitable emission of N_2O (300 kg of N_2O per ton of adipic acid), leading to global warming and ozone depletion [3,5–7]. Various technologies have been implemented to avoid the N_2O emissions, such as thermally decomposing it into O_2 and N_2, recovering N_2O to

prepare cyclododecanone via oxidation of cyclododecene, or to help hydroxylation of benzene to phenol [8–10].

Taking into account the atom economy and sustainable development as well as the compatibility of the downstream approaches and industrial practice, many efforts have been devoted to developing more efficient and eco-friendly processes for the industrial production of adipic acid that avoid the use of nitric acid [11–14]. Recently, alternative substrates for the green production of AA have been well investigated, including cyclohexane [11,13,15–17], cyclohexene [18–20], cyclohexanone, and cyclohexanol [21–27]. In 2014, Hwang and Sagadevan have reported a one-pot protocol to convert cyclohexane to adipic acid at room temperature by using ozone and UV light. However, the reaction is time-consuming (15 h) and the overall adipic acid yield (~75%) still needs to be improved [13]. Sato et al. have developed a biphasic system for the oxidation of cyclohexene to AA using 30% H_2O_2 in the presence of Na_2WO_4 as a homogeneous catalyst and $[CH_3(n-C_8H_{17})_3N]HSO_4$ as a phase-transfer catalyst [14]. The overall adipic acid yield (93%) is very high, but the industrial applicability of the phase-transfer catalyst is expensive, and the quaternary ammoniums cation also have a negative environmental impact [28]. In 2003, Usui and Sato subsequently discovered that 78% yield of AA could be achieved by oxidizing cyclohexanol (91% yield for cyclohexanone) with 30% H_2O_2 over H_2WO_4 at 90 °C for 20 h [27]. While some positive outcomes were obtained, the drastic reaction conditions, the demand of phase transfer catalyst, high-energy consumption, and the low yields of AA restricted their industrial applications. Thus, an efficient, eco-friendly, and low energy consumption route to AA from cyclohexanone with solvent free is highly desirable.

Polyoxometalates (POMs) have been well applied in catalysis owing to their structural diversity and fascinating properties, including tunable acidity and redox properties, inherent resistance to oxidative decomposition, high thermal stability, and impressive sensitivity to light and electricity [29–31]. Recently, Zhong and Yin et al. have synthesized a novel hollow-structured Mn-HTS catalyst to catalyze the oxidative cleavage of cyclohexanone for AA production [22]. The Mn species in Mn-HTS are presumably responsible for the production of radical intermediates to increase the reaction rate and contribute to the tautomerism between cyclohexanone and the corresponding enolic form [16,22]. In addition, POMs could not only serve as co-catalysts but could stabilize the active metal sites and regulate the electronic structure of catalysts to give rise to the enhancement of catalytic activities [32–35]. Over the years, our group has dedicated substantial efforts on the development of organically functionalized Anderson-type POMs [30,36–43]. Thus, we predicted that the Anderson-type POMs with manganese as the active metal site might catalyze the green oxidation of cyclohexanone, cyclohexanol, and KA oil to AA with high reactivity. Herein, a triol-functionalized butterfly-shaped β isomer of Mn(III)–Anderson POMs nanocluster, β-$\{[H_3NC(CH_2O)_3]_2MnMo_6O_{18}\}^-$ (**1**), has been synthesized and served as a catalyst for the selective oxidation of KA oil to AA with atom economy use of 30% H_2O_2 under solvent-free and room-temperature (without heating) conditions (Scheme 1). This route will greatly reduce the energy consumption and will provide a new perspective for the design of highly active catalysts for the green AA production.
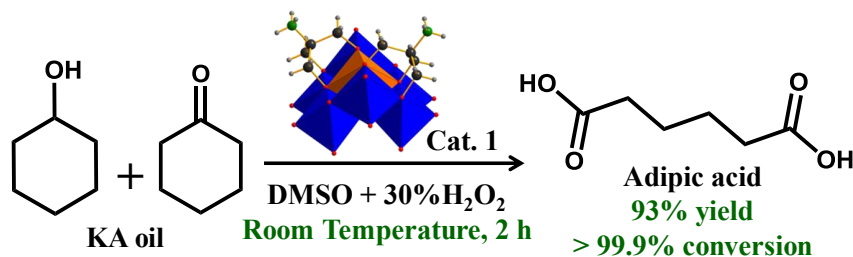

Scheme 1. One-pot selective oxidation of KA oil (cyclohexanone and cyclohexanol mixture with a mole ratio of 2:1) towards adipic acid catalyzed by β-$\{[H_3NC(CH_2O)_3]_2MnMo_6O_{18}\}^-$ (**1**). Colour code: Mo, blue; Mn, orange; O, red; N, green; C, black; H, gray.

2. Results and Discussion

2.1. The Structure Characterizations of Catalyst *1*

The POMs-based catalyst **1** was synthesized by a reaction of flat Anderson–Evans POMs cluster, α-$[Mn(OH)_6Mo_6O_{18}]^{3-}$, and triol ligands in hot (DMF) under N_2 atmosphere (details see experiment part in SI). Single crystal XRD analysis revealed that catalyst **1**, $[NH_4]$ β-$\{[H_3NC(CH_2O)_3]_2MnMo_6O_{18}\}$, crystallizes in the monoclinic space group C2/c (Table S1) and possesses a butterfly-shaped β-Anderson POM nanocluster (ca. 0.88 nm) with Mn^{3+} metal ion as the central heteroatom, and stabilized by two tris ligands (Figure 1a). Selected bond lengths of catalyst **1** are listed in Table S2. The anion nanocluster **1** and counter cations, NH_4^+, pack together and further assemble into a porous supermolecule structure with 4.47 Å × 11.68 Å nanopores *via* intermolecular hydrogen bonding and electrostatic interaction (Figure 1b,c, Table S3).
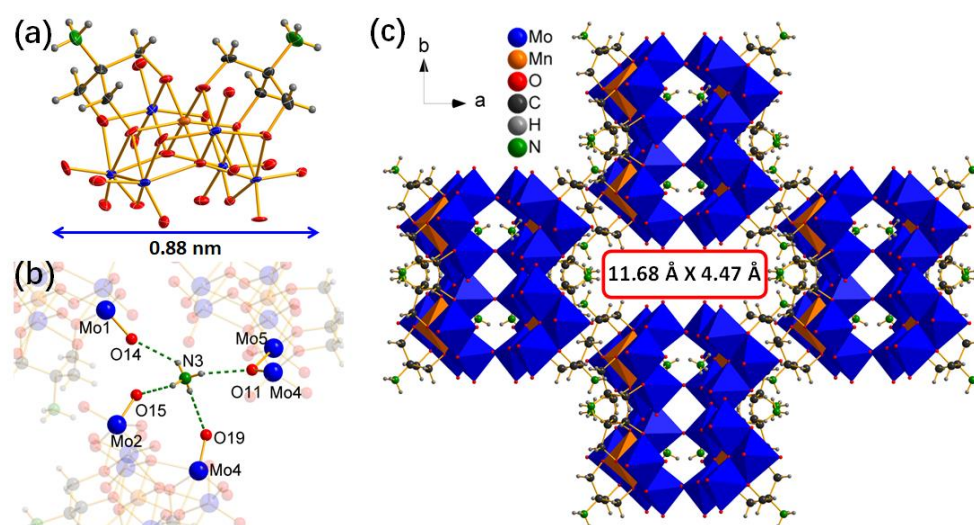
Figure 1. Structures of catalyst **1**. (**a**) ORTEP drawing of nanocluster **1** (30% probability ellipsoid); (**b**) Hydrogen bonding interactions between NH_4^+ and nanocluster **1**; (**c**) The crystal structure of catalyst **1** packing along *c* axis.

Powder XRD, IR, UV-Vis, ESI-MS, and ^{13}C NMR analyses were also conducted to characterize catalyst **1** (Figure 2 and Figures S1–S3). Firstly, the phase purity of catalyst **1** was characterized by powder X-ray diffraction and IR spectroscopy. The powder XRD pattern of catalyst **1** was almost identical to the simulated powder XRD pattern from the single crystal XRD result, confirming the phase purity as well as the excellent crystallinity of catalyst **1** (Figure 2a). As shown in Figure 2b, the characteristic peaks at 937, 919, and 897 cm^{-1} could be assigned to the vibrations of terminal Mo=O units and those at 790, 737, and 661 cm^{-1} belonged to the vibrations of the Mo–O–Mo groups. The characteristic peaks at 1117, 1054, and 1027 cm^{-1} could be assigned to the vibration peaks of the C–O bonds which demonstrated the grafting of tris onto the surface of β isomeric Anderson cluster. Notably, the splitting of three C–O bonds could be attributed to the fact that there exist three types of C–O bonds: one type of (μ_3–O)–C bonds and two types of (μ_2–O)–C.
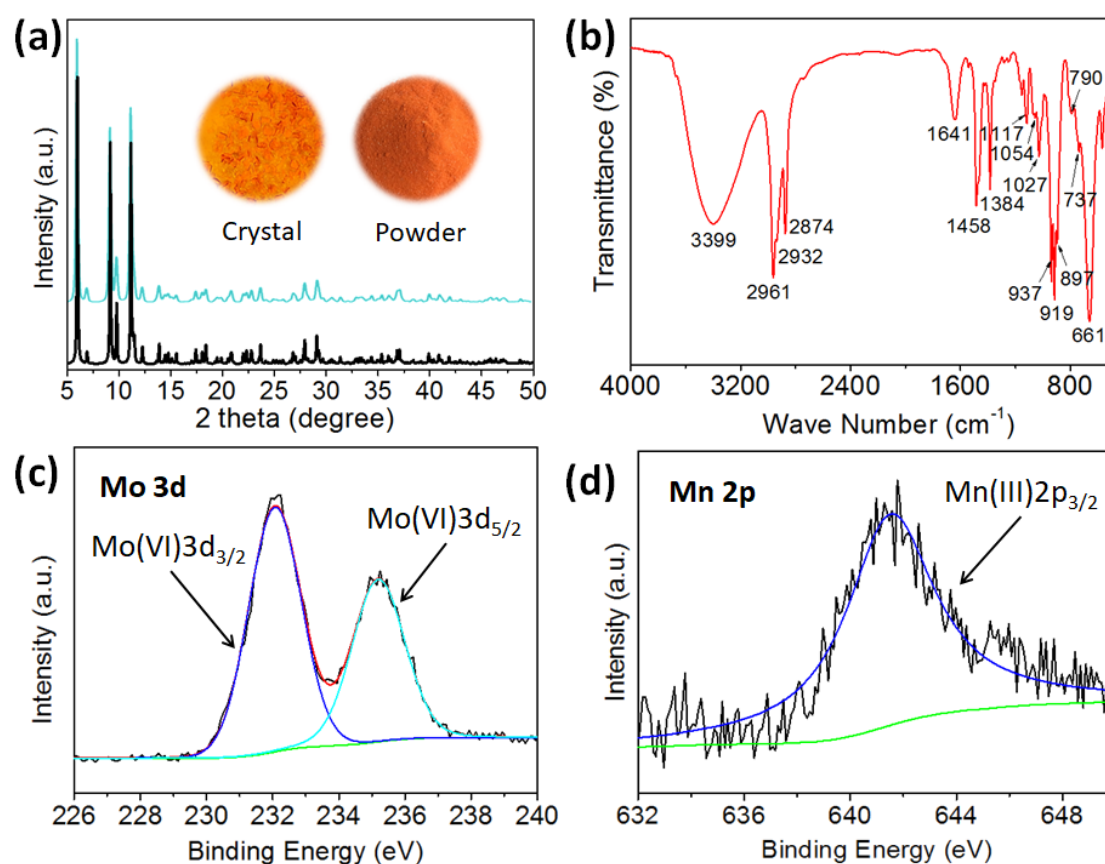
Figure 2. (**a**) XRD patterns (inset: digital photos, crystal and powder) of catalyst **1** (black, simulated XRD pattern of single crystal XRD of catalyst **1**; blue, powder XRD pattern of compound **1**); (**b**) The IR spectrum of catalyst **1**; (**c,d**) The XPS spectra of (**c**) Mo3d and (**d**) Mn2p for catalyst **1**.
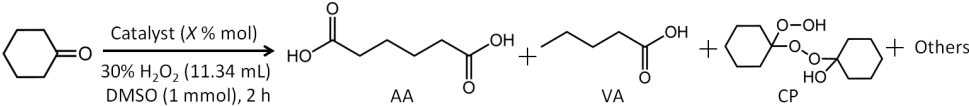
The X-ray photoelectron spectroscopy (XPS) in Figure 2c,d showed that catalyst **1** possessed binding energy (BE) around 232 eV and 235 eV belonging to Mo(VI) 3d3/2 and Mo(VI) 3d5/2 of Mo^{6+} species, respectively. Moreover, the binding energies in the intervals around 641 eV can be attributed to Mn 2p3/2, indicating the presence of Mn^{3+} ions on the surface of catalyst **1** [22]. Since many Mn species have been demonstrated as excellent catalysts for the synthesis of AA [16,22,23,25], such a butterfly-shaped Mn(III)–Anderson POM nanocluster may potentially allow a combination of the function of Mn and POM catalysts to achieve a synergistic catalysis for the AA production.

2.2. Cyclohexanone Oxidation Reaction

In our initial experiments, direct oxidation of cyclohexanone to AA was performed as a model reaction to screen the reaction conditions, and the results are listed in Table 1. As expected, the reaction did not occur without any catalysts (entry 1 in Table 1). The catalyst **1** showed cyclohexanone conversion of >99.9% and AA selectivity of 97.1% in the presence of 0.02 mol % catalyst **1** after 2 h (entry 2 in Table 1). Moreover, the as-prepared AA could be isolated as white crystalline products from the solution after cooling at −5 °C for 12 h, whose melting point is ca. 152.4 °C. The reaction solution was further analysed by ESI-MS, indicating that AA was the major product with 100% intensity at m/z = 145.04, and only a few valeric acid as by-product was formed (Figure S4). Then, ^1H and ^{13}C NMR spectra (in [D_6] DMSO) were applied to characterize the purity of the as-prepared AA crystal products (Figure S5). Control experiments showed that altering the catalyst loading had little influence on the product yield (entries 2–6 in Table 1). Regarding the oxidant, in this cyclohexanone to AA oxidization reaction, 1 mol AA generation will consume about 3.3 mol H_2O_2, which is much less

compared with the previous protocol developed by Noyori, in which 1 mol AA generation per 4.5 mol H_2O_2 consumption [13]. Upon decreasing the amount of H_2O_2, the yield of AA dropped significantly (entry 7 in Table 1).

Table 1. Cyclohexanone oxidation with H_2O_2 over catalysts. [1]

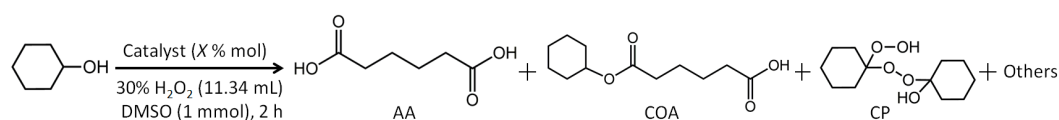| Entry	Cat.	mol % Cat.	Conv. % [2]	TOF h^{-1}	Yield % AA	Selectivity % [3]			
						AA	VA	CP	Others
1	Blank	0	1.6	-	0	-	-	>99.9	-
2	1	0.02	>99.9	14775	97.1	97.1	2.9	-	-
3	1	0.01	98.5	14775	95.9	97.4	2.6	-	-
4	1	0.04	>99.9	14775	96.8	96.8	3	-	0.2
5	1	0.08	>99.9	14775	96.5	96.5	2.5	-	1
6	1	0.1	>99.9	14775	96.4	96.4	2.2	-	1.4
7 [4]	1	0.02	46.8	14775	45.7	97.6	2.4	-	-
8 [5]	1	0.02	>99.9	14775	97.2	97.2	2.8	-	-
9	Na_2MoO_4	0.02	24.7	3705	28.9	11.7	-	88.3	-
10	$(NH_4)_6Mo_7O_{24}$	0.02	35.9	5385	52.1	14.5	-	85.5	-
11	$Mn(CH_3COO)_2$	0.02	2.5	375	1.59	63.5	23.7	-	12.8
12	$[NH_4]_3 \cdot \alpha$-$[Mn(OH)_6Mo_6O_{18}]$	0.02	67.4	10110	46.4	68.9	-	31.1	-

[1] Conditions: catalyst (0.02 mol %), 30% H_2O_2 (100 mmol), DMSO (1 mmol), and cyclohexanone (30 mmol), in an unsealed reactor with reflux condensing tube and magnetic stirring unless otherwise noted. [2] Cyclohexanone conversion based on cyclohexanone consumed. [3] Product selectivity = content of this product/the cyclohexanone consumed; AA: adipic acid; VA: valeric acid; CP: cyclohexanone peroxide; others: probably CO_2. [4] 30% H_2O_2 (50 mmol) was used instead. [5] Reaction was carried out without DMSO additive.

With respect to active centers, detailed comparisons (Table 1, entries 9 and 10) with other catalysts such as Na_2MoO_4, $(NH_4)_6Mo_7O_{24}$ leave no doubt that the active sites in our highly active catalyst **1** is the special central Mn^{3+} species. Furthermore, only few AA product could be obtained using simple manganese salts as catalyst, $Mn(CH_3COO)_2$ (entry 11 in Table 1). The catalytic activity of common flat Anderson-type POMs with Mn(III) as central heteroatom is higher than that of $(NH_4)_6Mo_7O_{24}$ and Na_2MoO_4, indicating that Mn^{3+} species are more active than Mo^{6+} species (entry 12 in Table 1). Furthermore, the catalytic property of catalyst **1** was better than that of common flat Anderson-type POMs with Mn(III) as the central heteroatom (entries 2 and 12 in Table 1). Based on the above results, it can be inferred that both the special butterfly-shaped topology and the chemical environment of Mn^{3+} central atom in catalyst **1** are key factors to the high performance of catalytic oxidation of cyclohexanone to AA. Moreover, analyses of the H_2O_2 degradation over these different catalysts revealed that simple manganese salts, $Mn(CH_3COO)_2$, could result in the rapid decomposition of H_2O_2, and thus lead to low catalytic activity, while for catalyst **1**, Na_2MoO_4, $(NH_4)_6Mo_7O_{24}$, and $[NH_4]_3 \cdot \alpha$-$[Mn(OH)_6Mo_6O_{18}]$ catalysts, the H_2O_2 degradation rate could be ignored. It should be noted that in such a green AA production, both catalyst **1** and H_2O_2 were essential to the high performance of oxidative catalytic activity. Of note, the valance state of reference catalysts including $Mn(CH_3COO)_2$, Na_2MoO_4, $(NH_4)_6Mo_7O_{24}$, and $[NH4]_3 \cdot \alpha$-$[Mn(OH)_6Mo_6O_{18}]$ were clear. The valance state of Mo in these reference catalysts was also Mo^{6+} and the valance state of Mn in $[NH4]_3 \cdot \alpha$-$[Mn(OH)_6Mo_6O_{18}]$ was also Mn^{3+}. It is likely that such high catalytic oxidation performance may be attributed to the special butterfly-shaped topology of β-$\{[H_3NC(CH_2O)_3]_2MnMo_6O_{18}\}$, leading to the specific chemical environment of Mn^{3+} central atom in catalyst **1**, since the butterfly-shaped topology of β-$\{[H_3NC(CH_2O)_3]_2MnMo_6O_{18}\}$ makes the Mn^{3+} central atom more "uncovered" as the active site by the comparison with the flat topology of α-$[Mn(OH)_6Mo_6O_{18}]$ (Figure S6). For the organoimidization functionalized POM derivatives, the aromatic segment was directly linked on the POM cluster through the Mo≡N bond, thus the conjugated electron of organic ligands obviously enriched the POM nanocluster through delocalization [30]. However, for the alkoxylation modification of the Anderson

nanocluster, organic ligand electronic-driven effect was not obvious and can be ignored, as only slight electronic depletion that cause hypsochromic shift was observed, as we investigated before [38]. Hence, the triol ligand just plays an important role in stabilizing β-{[$H_3NC(CH_2O)_3$]$_2MnMo_6O_{18}$} as the specific butterfly-shaped topology according to the DFT calculations we reported before [37].

In order to further understand the relationship between the reaction selectivity, conversion, and reaction conditions in such catalytic oxidation, we investigated the effect of reaction parameters. The reaction selectivity and conversion versus reaction temperature, time, and catalyst amounts were further investigated to optimize the reaction condition. The catalyst shows a low activity with 100% AA selectivity at 5 °C, but with increasing temperature the conversion of cyclohexanone increased. At 25 °C (room temperature), we found that the formation of AA was optimum with both desirable selectivity and conversion. However, with continuous increase of temperature to 100 °C, the conversion of cyclohexanone slightly increased but the AA selectivity significantly decreased. This may be due to the fact that the butterfly-shaped Mn(III)–polyoxometalate nanocluster was a high reactivity catalysis and the H_2O_2 was also a strong oxidant, leading to the continuous and over-oxidization of AA towards other products under the elevated temperatures. The catalyst shows a low cyclohexanone conversion with 100% AA selectivity at the very beginning of the reaction. With the increasing time, the conversion of cyclohexanone increased but adipic acid selectivity decreased slightly. At about 1.7 h, we found that the formation of AA was optimum with both desirable selectivity and conversion of 97.8%. However, after 2 h, the selectivity significantly decreased and the prolongation of reaction time will cause the over-oxidization and the decomposition of AA. (Figure S7). In addition, the optimum reaction temperature and time were determined to be 2 h at 25 °C. Based on the optimum reaction time, all the Turnover Frequency(TOF) in the entry of Tables 1 and 2, which indicated the intrinsic catalytic activities of these catalysts was further determined in the beginning of the reaction time (0.1 h) with low conversion under 10%.

Table 2. Cyclohexanol oxidation with H_2O_2 over catalysts. [1]

Entry	Cat.	mol % Cat.	Conv. % [2]	TOF h⁻¹	Yield % AA	Selectivity % [3]			
						AA	COA	CP	Others
1	Blank	0	0.5	-	0	-	-	-	>99.9
2	1	0.02	>99.9	13257	85.3	85.3	8.3	6.4	-
3	1	0.01	98.2	13257	84.9	86.5	7.9	5.6	-
4	1	0.04	>99.9	13257	85.8	85.8	6.4	7.8	-
5	1	0.08	>99.9	13257	85.9	85.9	5.8	8.3	-
6	1	0.1	>99.9	13257	85.4	85.4	5.2	9.4	-
7 [4]	1	0.02	0.1	13.5	0	-	-	-	>99.9
8 [5]	1	0.02	45.8	13257	40.3	88.1	2.9	3.7	5.3
9 [6]	1	0.02	21.4	2889	13.7	64	-	29.2	6.8
10 [7]	1	0.02	85.7	11569.5	40	87.5	4.8	5.6	2.1
11 [8]	1	0.02	46.7	13257	26.2	56.2	2.8	1.5	39.59
12	Na₂MoO₄	0.02	12.2	1647	1.15	9.4	4.1	86.5	-
13	(NH4)₆Mo₇O₂₄	0.02	18.4	2484	2.32	12.6	4.5	82.9	-
14	Mn(CH₃COO)₂	0.02	3.1	418.5	1.65	53.3	23.7	-	14
15	[NH4]₃·α-[Mn(OH)₆Mo₆O₁₈]	0.02	53.7	7249.5	41.6	77.4	12.3	10.3	-

[1] Conditions: catalyst (0.02 mol %), 30% H_2O_2 (100 mmol), DMSO (1 mmol), and cyclohexanol (23 mmol), in an unsealed reactor with reflux condensing tube and magnetic stirring unless otherwise noted. [2] Cyclohexanol conversion based on cyclohexanol consumed. [3] Product selectivity = content of this product/the cyclohexanol consumed; AA: adipic acid; COA: 6-(cyclohexyloxy)-6-oxohexanoic acid; CP: cyclohexanone peroxide; others: probably CO_2, cyclohexanone or 6-oxohexanoic acid et al. [4] Reaction was carried out without H_2O_2. [5] 30% H_2O_2 (50 mmol) was used instead. [6] Reaction was carried out without DMSO. [7] Reaction was carried out with 5 mmol DMSO. [8] Reaction time was 0.5 h. Yield of cyclohexanone is 37.8%, determined by gas chromatography using chlorobenzene as the internal standard.

2.3. Cyclohexanol Oxidation Reaction

From the viewpoint that some practical AA production starts from cyclohexanol, herein, we have also studied the oxidization of cyclohexanol towards AA in the presence of catalyst **1** (Table 2). The reaction was conducted as the following: catalyst **1** (5.4 mg, 4.6×10^{-6} mol), DMSO (1 mmol), 30% H_2O_2 (100 mmol), and cyclohexanol (23 mmol) were mixed and stirred in unsealed reactor with reflux condensing tube without extra heating. After 2 h, cyclohexanol conversion of >99.9% and AA selectivity of 85.3% could be obtained. However, the ESI-MS result shows that few byproduct species contained valeric acid ($m/z = 101.06$), 6-(cyclohexyloxy)-6-oxohexanoic acid ($m/z = 229.14$) (Figure S8) were observed. Experiments showed that the catalyst loading had little influence on the product yield, but if without catalyst or H_2O_2, AA products could not be obtained (Table 2, entries 1–7 in Table 2). The yield of AA dropped significantly when the amount of H_2O_2 decreased (entry 8 in Table 2). As shown in entry 8 of Table 1, DMSO almost has no influence on the cyclohexanone oxidation reaction towards AA. However, in the case of cyclohexanol oxidation, only low yield of AA (13.7%) could be obtained if without DMSO (entry 9 in Table 2), while an excess addition of DMSO results in the reduction of AA yield (40.0% yield, entry 10 in Table 2) since DMSO could also react with H_2O_2 to form methyl sulfone, leading to an additional consumption of H_2O_2, where the remaining H_2O_2 cannot make cyclohexanol completely converted into AA, and thus an incomplete oxidation byproduct 6-oxohexanoic acid instead (Figure S9). Furthermore, we found that 37.8% yield of cyclohexanone could be obtained after 0.5 h, indicating that cyclohexanol was firstly oxidized into cyclohexanone. From entry 9 and entry 11 in Table 2, we may consider that DMSO is the co-catalyst for the oxidation of cyclohexanol into cyclohexanone. The generated cyclohexanone could be easily converted into AA product selectively in the presence of catalyst **1** and H_2O_2 (Table 1).

Compared with Tables 1 and 2, the decrease of AA yield from catalytic oxidation of cyclohexanol could be observed, which can be explained by the fact that the rate of alcohol oxidation to AA is lower than that of ketone.[23] With respect to active centers, detailed comparisons with other catalysts including Na_2MoO_4, $(NH_4)_6Mo_7O_{24}$, and $[NH_4]_3 \cdot \alpha$-$[Mn(OH)_6Mo_6O_{18}]$ leave no doubt that the active site is Mn^{3+} center in the special butterfly-shaped topology of catalyst **1** (entries 9–12 in Table 1, entries 12–15 in Table 2).

## 2.4. KA Oil Oxidation Reaction and Catalyst Recyclability

Since compound **1** has been demonstrated as a highly active catalyst for the selective oxidation of both cyclohexanone and cyclohexanol towards AA production (Tables 1 and 2), we assumed that the catalytic oxidation of KA oil (a mixture of cyclohexanone and cyclohexanol) towards AA could be achieved in the presence of catalyst **1**. As shown in Table 3, the influence of cyclohexanone (-one) and cyclohexanol (-ol) mixtures with various ratios on the AA yield has also been studied. In the absence of cyclohexanone, the AA yield is 84%. The increase of the percentage of cyclohexanone from 20 to 100% in the reaction mixture led to an increase of AA yield from ca. 88 to 98%, which is in accordance with the above results (Tables 1 and 2). According to the 2:1 ratio of cyclohexanone and cyclohexanol in the current industrial KA oil, a reaction catalyzed by compound **1** was conducted to simulate current industrial AA production line from KA oil as follows: catalyst **1** (7.0 mg, 6×10^{-3} mmol), DMSO (1 mmol), 30% H_2O_2 (100 mmol), cyclohexanol (10 mmol), and cyclohexanone (20 mmol) were mixed and stirred at room temperature. After 2 h, pure AA product could be obtained with 93% yield. The above results demonstrated that the selectively catalytic oxidation of KA oil could be achieved by catalyst **1.**

Table 3. Catalytic oxidation of various cyclohexanone/cyclohexanol mixtures towards AA over catalyst **1**. [1]

Substrate (one/ol)	0/10	2/8	4/6	6/4	2/1	8/2	10/0
Yield %	84	88	90	92	93	95	98

[1] Conditions: catalyst (0.02 mol %), 30% H_2O_2 (120 mmol), DMSO (1 mmol), and cyclohexanone/cyclohexanol (30 mmol), unless otherwise noted.

The recycle ability of catalyst **1** was further tested by reusing the reaction solution, which was rotary evaporated and concentrated to 2 mL at low temperature of 50 °C. Of note, suitable sacrificial reductant Na_2SO_3 was added to eliminate the possible residual H_2O_2 before the evaporation operation, though according to the almost atom economy use of H_2O_2 catalytic reaction protocol, the residual H_2O_2 would not be very high. With this safety precaution, the safety of the whole catalyst cycling process would be guaranteed (Figure 3). Fresh 30% H_2O_2 (120 mmol) and substrates (20 mmol cyclohexanone and 10 mmol cyclohexanol) were added into the reaction each recycle run. AA products can still be obtained with good yield and high selectivity. However, an appreciable loss of catalytic ability of catalyst **1** (approaching to 88% AA yield) was observed after three runs, indicating fewer catalyst deactivation during catalysis. A total Turnover Number (TON) of 20,900 could be achieved over catalyst **1** after five runs. Moreover, a high TOF of 2325 h^{-1} could also be obtained in the first run with catalyst **1**.
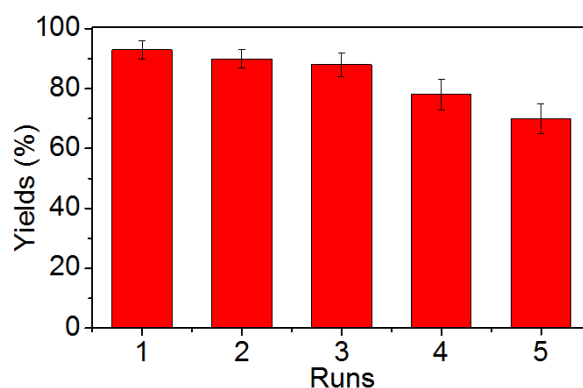
Figure 3. Recyclability tests of catalyst **1** for the KA oil oxidation towards AA with 30% H_2O_2. Conditions: catalyst **1** (0.02 mol %), 30% H_2O_2 (120 mmol), DMSO (1 mmol), cyclohexanone (20 mmol), and cyclohexanol (10 mmol), room temperature for 2 h.

3. Materials and Methods

3.1. General Methods and Materials

All syntheses and manipulations were performed in the open air. The $[MnMo_6O_{18}(OH)_6]^{3-}$ was synthesized according to literature methods [44]. All other chemicals including solvents were commercially available as reagent grade and used as received without further purification from Adamas-beta® (Shanghai, China). IR spectrum was measured using KBr pellets and recorded on a Perkin Elmer FT-IR spectrometer. UV-Vis spectrum was measured in acetonitrile solution by Agilent Cary 300 spectrophotometer (Agilent Technologies Inc., San Francisco, CA, USA). The mass spectrum was obtained using an ion trap mass spectrometer (Thermofisher LTQ, Waltham, MA, USA). Negative mode was chosen for the experiments (capillary voltage 33 V). Sample solution (in acetonitrile) was infused into the ESI source at a flow rate of 300 µL min^{-1}. ^1H and ^{13}C NMR spectra were obtained on a JEOL JNM-ECA400 spectrometer and are reported in ppm (JEOL Ltd., Tokyo, Japan). Elemental analyses of C, H, and N were performed by Elementar Analysensysteme GmbH (Elementar Analysensysteme GmbH, Langenselbold, Germany) while the Elemental analyses of Mn and Mo were

performed by X-ray fluorescence (XRF) element analyzer PANalytical Epsilon 5 (PANalytical B.V., Almelo, The Netherlands). Thermal gravimetric analysis (TGA) measurements were performed on a Mettler Toledo TGA/SDTA851 (Mettler-Toledo group, Zurich, Switzerland) in flowing Ar 50.0 mL/min with a heating rate of 20 K/min. XPS measurements were performed under ultrahigh vacuum (UHV) with 1.0×10^{-7} Torr, axis HS monochromatized Al Kα cathode source at 150 W, focused X-ray 100 μm beam, pass energy: 55 eV wih 0.1 ev step length, detect angle (take off): 45° on X-ray microprobe (ULVAC-PHI Quantera SXM, Ulvac-Phi Ltd., Chigasaki, Kanagawa, Japan). Binding energy was calibrated with C1s = 284.8 eV. The powder product was measured by PANalytical X'Pert (PANalytical B.V., Almelo, The Netherlands). Powder X-ray powder diffractometer operated at a voltage of 60 kV and current of 55 mA with CuKα radiation (λ = 1.5406 Å) (PANalytical B.V., Almelo, The Netherlands). Gas chromatography (GC) (Shimadzu Ltd., Kyoto, Japan) was performed on Shimadzu GC-2010 Plus equipped with an RTX-5 (30 m × 0.25 mm × 0.25 μm) column and FID detector for liquid phase analysis (GC conditions: injector temperature: 240 °C; detector temperature: 250 °C, oven temperature: 50–180 °C with heating rate of 10 °C min^{-1}; carrier: helium; column flow: 4 mL min^{-1}; linear velocity: 37 cm s^{-1}) or a Carboxen®-1010 PLOT (15 m × 0.25 mm × 0.25 μm) Capillary GC Column and BID detector (Shimadzu Ltd., Kyoto, Japan) for gas phase analysis (GC conditions: injector temperature: 230 °C; detector temperature: 235 °C, oven temperature: 26 °C; carrier: helium; column flow: 5 mL min^{-1}; linear velocity: 77 cm s^{-1}). High performance liquid chromatograph (HPLC) (Agilent Technologies Inc., San Francisco, CA, USA.) was performed on an Agilent 1290 series HPLC instrument with a HYPERSIL BDS inverse phase C$_{18}$ column (250 mm × 4.6 mm × 5 μm), operating at room temperature. The solid mixtures were separated and dried at 70 °C in vacuum for 24 h and finally dissolved in methanol and identified by HPLC-MS with 15:75:10 (*v/v*) of CH$_3$OH:H$_2$O:KH$_2$PO$_4$ as mobile phase, detected at 210 nm of wavelength and 1.0 mL/min of flow, and quantified by HPLC external standard calibration curve method.

3.2. The Synthesis of (NH$_4$)$_3$[Mn(OH)$_6$Mo$_6$O$_{18}$] and [TBA]$_3$[Mn(OH)$_6$Mo$_6$O$_{18}$]

(NH$_4$)$_3$[Mn(OH)$_6$Mo$_6$O$_{18}$] was obtained according to literature methods [44]. Then it was precipitated from the aqueous solution to exchange the counter-cation of (NH$_4$)$^+$ with TBA$^+$ by adding equivalent amount of [TBA]Br. C$_{48}$H$_{114}$N$_3$MnMo$_6$O$_{24}$, M$_r$ = 1748.02, H 6.50 C 32.85 N 2.35 Mn 3.00 Mo 32.66 while calcd H 6.57 C 32.98 N 2.40 Mn 3.14 Mo 32.93. IR (KBr pellet, major absorbance, cm^{-1}): 3147, 1402, 937, 890, 814, 792, 697. UV-Vis (MeCN, nm): λ_{LMCT} = 230 (ε_{LMCT} = 5.31 × 10^5 L·mol^{-1}·cm^{-1}), $\lambda_{d\text{-}d}$ = 477 ($\varepsilon_{d\text{-}d}$ = 6.14 × 10^2 L·mol^{-1}·cm^{-1}).

3.3. The Synthesis of Compound **1**

A mixture of [TBA]$_3$[Mn(OH)$_6$Mo$_6$O$_{18}$] (1.748 g 1 mmol) with tris(hydroxymethyl)-aminomethane (0.242 g, 2 mmol) was dissolved in 25 mL hot DMF. After being heated for 12 h under nitrogen gas, the reaction solution was cooled down to room temperature to remove the precipitates by filtration and a dark orange solution was obtained. Then the filtrate was poured into ether, resulting in precipitation. After the solution became clear, the supernatant liquid was poured off. The product was obtained as dark orange powders (49% yield based on Mo). C$_{56}$H$_{124}$N$_5$MnMo$_6$O$_{24}$ M$_r$ = 1882.20, H 6.50 C 35.66 N 3.65 Mn 2.89 Mo 30.49 while calcd H 6.64 C 35.74 N 3.72 Mn 2.92 Mo 30.58. IR (KBr pellet, major absorbance, cm^{-1}): 3399, 2961, 2932, 2874, 1641, 1458, 1384, 1117, 1054, 1027, 937, 919, 897, 790, 737, 661. UV-Vis (MeCN, nm): λ_{LMCT} = 212, (ε_{LMCT} = 7.42 × 10^5 L·mol^{-1}·cm^{-1}) $\lambda_{d\text{-}d}$ = 461 ($\varepsilon_{d\text{-}d}$ = 8.53 × 10^2 L·mol^{-1}·cm^{-1}). ESI-MS (MeCN): calcd *m/z* = 1639.73 (TBA)$_2$\{[H$_2$NC(CH$_2$O)$_3$]$_2$MnMo$_6$O$_{18}$\}$^-$, 1398.26 [H$^+$](TBA) \{[H$_2$NC(CH$_2$O)$_3$]$_2$MnMo$_6$O$_{18}$\}$^-$, 698.63 (TBA)$_1$\{[H$_2$NC(CH$_2$O)$_3$]$_2$MnMo$_6$O$_{18}$\}$^{2-}$, 577.89 [H$^+$]\{[H$_2$NC(CH$_2$O)$_3$]$_2$MnMo$_6$O$_{18}$\}$^{2-}$, 384.93 \{[H$_2$NC(CH$_2$O)$_3$]$_2$MnMo$_6$O$_{18}$\}$^{3-}$; found 1639.62, 1397.88, 698.48, 577.55, 384.72 respectively. ^{13}C NMR (400 MHz, [D$_6$] DMSO, ppm): δ = 13.8 (C$_\alpha$), 19.0 (C$_\beta$), 23.5 (C$_\gamma$), 57.8 (C$_\varepsilon$), 60.8 (C$_a$), 63.9 (C$_b$), 68.3 (C$_c$), 72.8 (C$_d$). The crystallization of catalyst **1**: [NH$_4$]H$_2$\{[H$_2$NC(CH$_2$O)$_3$]$_2$MnMo$_6$O$_{18}$\}, C$_8$H$_{22}$N$_3$MnMo$_6$O$_{24}$, M$_r$ = 1174.84. 1 g

$(TBA)_3\{[H_2NC(CH_2O)_3]_2MnMo_6O_{18}\}$ were redissolved in 5 mL MeCN, additional 0.1 g of NH_4Cl was dissolved into 1 mL 0.1 M HCl then added into the crystallization solution to accelerate crystallization process. Single crystals suitable for X-ray diffraction were grown in MeCN solvent by slow evaporation. After crystallization, catalyst **1** was obtained as dark orange crystalline product. Elemental analysis: Mn 4.71, Mo 48.98 while calcd. Mn 4.68, Mo 49.00.

3.4. Cyclohexanone, Cyclohexanol, and KA Oil Oxidation

The catalytic oxidation of cyclohexanone was carried out in an unsealed reactor with reflux condensing tube and magnetic stirring. In a typical experiment, catalyst **1** (0.02 mol %), 30% H_2O_2, DMSO, and reaction substrates (cyclohexanone, cyclohexanol, or KA oil) were mixed together and reacted under room temperature without extra heating. After the reaction, the mixture was cooled down, dissolved in ice water, and filtered. The solid mixtures were separated and dried at 70 °C in vacuum for 24 h and finally dissolved in methanol and identified by HPLC-MS with 15:75:10 (*v/v*) of $CH_3OH/H_2O/KH_2PO_4$ as mobile phase, detected at 210 nm of wavelength and 1.0 mL/min of flow, and quantified by HPLC external standard calibration curve method. The liquid phase was analyzed by Shimadzu GC-2010 Plus equipped with an RTX-5 (30 m × 0.25 mm × 0.25 μm) column and chlorobenzene was utilized as the internal standard. The components of gas phase were analyzed by GC equipped with a Carboxen®-1010 PLOT (15 m × 0.25 mm × 0.25 μm) Capillary GC Column and BID detector.

3.5. X-ray Crystallography

Suitable single crystal was selected. Data collection was performed by graphite-monochromated Mo-Kα radiation (λ = 0.71073 Å). Data reduction, cell refinement and experimental absorption correction were performed with the software package of Agilent Gemini Ultra CrysAlisPro (Ver 1.171.35.11) (Agilent Technologies Inc., San Francisco, CA, USA). Structures were solved by intrinsic phasing and refined against F^2 by full-matrix least-squares. All non-hydrogen atoms were refined anisotropically. All calculations were carried out by the program package of SHELXT and Olex2 ver 1.2.8 [45–47].

Crystallographic data for catalyst **1** is shown in Table S1. Atomic coordinates for the reported crystal structure has been deposited with the Cambridge Structural Database under the accession codes 1447786 for catalyst **1**. The data can be obtained free of charge from The Cambridge Crystallographic Data Centre via www.ccdc.cam.ac.uk/data_request/cif.

4. Conclusions

In conclusion, we have discovered a Mn^{3+} central β isomer of the well-known flat Anderson heteropolyanions, which possesses butterfly-shaped topology like $[Mo_7O_{24}]^{6-}$. We found that such organically derivatized butterfly-shaped Mn(III)–Anderson POMs can serve as catalyst for selective oxidation of cyclohexanone and cyclohexanol towards AA production with high yield and selectivity at room temperature (without heating). The AA production under room temperature would greatly reduce the energy consumption. The efficient utilization of 30% H_2O_2 as clean oxidant would eliminate N_2O emission. Catalytic system also worked for KA oil, which is highly desired in industrial "green" AA production. The above results indicated that such "green" AA synthesis is competitive and eco-friendly, and it is promising for the future AA production. Such an atom active site engineering in topology-controlled POMs catalyst described here provides a new perspective on the development of highly active catalysts for the adipic acid production.

Supplementary Materials: The following are available online at http://www.mdpi.com/2073-4344/8/3/121/s1, Table S1. Crystallographic data for compound **1**, Table S2. Selected bond lengths (Å) of cluster **1**, Table S3. Experimental hydrogen bonding interactions of compound **1**, Figure S1. (a) UV/Vis LMCT spectra of compound **1** and the flat Anderson-type POMs Cluster, $[MnMo_6O_{18}(OH)_6]^{3-}$. (b) UV/Vis d-d transition spectra of compound **1** and the flat Anderson-type POMs Cluster, $[MnMo_6O_{18}(OH)_6]^{3-}$, Figure S2. ^{13}C NMR spectrum of compound

1, Figure S3. (a) ESI-MS of compound **1** with TBA$^+$ cations. (b) ESI-MS of compound **1** with TBA+ cations (100% intensity peak in original size), Figure S4. (a) The ESI-MS of white crystalline products generated from cyclohexanone in the presence of catalyst **1**. (b)The HPLC retention time of white crystalline products dissolved in methanol. (c) The GC-MS of reaction solution dissolved in ethanol before catalytic reaction. (d) The GC-MS of reaction solution dissolved in ethanol after catalytic reaction, Figure S5. (a) ^{1}H NMR spectrum of white crystalline product. (b) ^{13}C NMR spectrum of white crystalline product, Figure S6. Topology analysis and comparison of Catalysis Species, Figure S7. (a) The reaction selectivity and conversion versus reaction temperature, reaction condition catalyst (0.02 mol %), 30% H_2O_2 (100 mmol), DMSO (1 mmol), and cyclohexanone (30 mmol) at 2 h. (b) The reaction selectivity and conversion versus time, reaction condition catalyst (0.02 mol %), 30% H_2O_2 (100 mmol), DMSO (1 mmol), and cyclohexanone (30 mmol) at 25 °C in cyclohexanone oxidation catalytic reaction, Figure S8. The ESI-MS of products from the catalytic oxidation of cyclohexanol at room temperature, Figure S9. The ESI-MS of white crystalline products generated from cyclohexanol with DMSO.

Author Contributions: Yongge Wei and Jiangwei Zhang conceived the project. Yichao Huang and Jianhui Luo co-wrote the manuscript. Jianhui Luo, Yichao Huang, Bin Ding, Pingmei Wang, Xiangfei Geng, and Jiangwei Zhang performed all the experiments. Yongge Wei helped improve the manuscript. Jiangwei Zhang conducted the X-ray Crystallographic Studies.

Conflicts of Interest: The authors declare no conflict of interest.

References

1. Davis, D.D.; Kemp, D.R. Adipic Acid. In *Kirk–Othmer Encyclopedia of Chemical Technology*, 4th ed.; Kroscwitz, J.I., Howe-Grant, M., Eds.; John Wiley & Sons, Inc.: New York, NY, USA, 1991; Volume 1, pp. 466–493, ISBN 9780471238966.

2. Wen, Y.; Wang, X.; Wei, H.; Li, B.; Jin, P.; Li, L. A large-scale continuous-flow process for the production of adipic acid via catalytic oxidation of cyclohexene with H_2O_2. *Green Chem.* **2012**, *14*, 2868–2875. [CrossRef]

3. Van de Vyver, S.; Román-Leshkov, Y. Emerging catalytic processes for the production of adipic acid. *Catal. Sci. Technol.* **2013**, *3*, 1465–1479. [CrossRef]

4. *Adipic Acid (ADPA), 2018 World Market Outlook and Forecast up to 2027*; Merchant Research and Consulting: Birmingham, UK, 2018.

5. Castellan, A.; Bart, J.C.J.; Cavallaro, S. Industrial production and use of adipic acid. *Catal. Today* **1991**, *9*, 237–254. [CrossRef]

6. Montzka, S.A.; Dlugokencky, E.J.; Butler, J.H. Non-CO_2 greenhouse gases and climate change. *Nature* **2011**, *476*, 43–50. [CrossRef] [PubMed]

7. Wu, M.; Fu, Y.; Zhan, W.; Guo, Y.; Guo, Y.; Wang, Y.; Lu, G. Catalytic Performance of MgO-Supported Co Catalyst for the Liquid Phase Oxidation of Cyclohexane with Molecular Oxygen. *Catalysts* **2017**, *7*, 155. [CrossRef]

8. Cavani, F.; Teles, J.H. Sustainability in Catalytic Oxidation: An Alternative Approach or a Structural Evolution? *ChemSusChem* **2009**, *2*, 508–534. [CrossRef] [PubMed]

9. Ivanov, D.P.; Kharitonov, A.S.; Piryutko, L.V. Phenol oxidation by nitrous oxide: The role of zeolite catalyst acidity. *Catal. Ind.* **2015**, *7*, 275–281. [CrossRef]

10. Zhang, R.; Hua, C.; Wang, B.; Jiang, Y. N_2O Decomposition over Cu–Zn/γ–Al_2O_3 Catalysts. *Catalysts* **2016**, *6*, 200. [CrossRef]

11. Ribeiro, A.P.C.; Martins, L.M.D.R.S.; Pombeiro, A.J.L. N_2O-Free single-pot conversion of cyclohexane to adipic acid catalysed by an iron(ii) scorpionate complex. *Green Chem.* **2017**, *19*, 1499–1501. [CrossRef]

12. Joo, J.C.; Khusnutdinova, A.N.; Flick, R.; Kim, T.; Bornscheuer, U.T.; Yakunin, A.F.; Mahadevan, R. Alkene hydrogenation activity of enoate reductases for an environmentally benign biosynthesis of adipic acid. *Chem. Sci.* **2017**, *8*, 1406–1413. [CrossRef] [PubMed]

13. Hwang, K.C.; Sagadevan, A. One-pot room-temperature conversion of cyclohexane to adipic acid by ozone and UV light. *Science* **2014**, *346*, 1495–1498. [CrossRef] [PubMed]

14. Sato, K.; Aoki, M.; Noyori, R. A "Green" Route to Adipic Acid: Direct Oxidation of Cyclohexenes with 30 Percent Hydrogen Peroxide. *Science* **1998**, *281*, 1646–1647. [CrossRef]

15. Dai, J.; Zhong, W.; Yi, W.; Liu, M.; Mao, L.; Xu, Q.; Yin, D. Bifunctional H_2WO_4/TS-1 catalysts for direct conversion of cyclohexane to adipic acid: Active sites and reaction steps. *Appl. Catal. B Environ.* **2016**, *192*, 325–341. [CrossRef]

16. Zou, G.; Zhong, W.; Xu, Q.; Xiao, J.; Liu, C.; Li, Y.; Mao, L.; Kirk, S.; Yin, D. Oxidation of cyclohexane to adipic acid catalyzed by Mn-doped titanosilicate with hollow structure. *Catal. Commun.* **2015**, *58*, 46–52. [CrossRef]

17. Acharyya, S.S.; Ghosh, S.; Bal, R. Nanoclusters of Cu(ii) supported on nanocrystalline W(vi) oxide: A potential catalyst for single-step conversion of cyclohexane to adipic acid. *Green Chem.* **2015**, *17*, 3490–3499. [CrossRef]

18. Vafaeezadeh, M.; Mahmoodi Hashemi, M. One pot oxidative cleavage of cyclohexene to adipic acid using silver tungstate nano-rods in a Bronsted acidic ionic liquid. *RSC Adv.* **2015**, *5*, 31298–31302. [CrossRef]

19. Vafaeezadeh, M.; Mahmoodi Hashemi, M. Simple and green oxidation of cyclohexene to adipic acid with an efficient and durable silica-functionalized ammonium tungstate catalyst. *Catal. Commun.* **2014**, *43*, 169–172. [CrossRef]

20. Ghosh, S.; Acharyya, S.S.; Adak, S.; Konathala, L.N.S.; Sasaki, T.; Bal, R. Selective oxidation of cyclohexene to adipic acid over silver supported tungsten oxide nanostructured catalysts. *Green Chem.* **2014**, *16*, 2826–2834. [CrossRef]

21. Ghiaci, M.; Hosseini, S.M.; Shahzeydi, A.; Martínez-Huerta, M.V. Oxidation of cyclohexanol to adipic acid with molecular oxygen catalyzed by ZnO nanoparticles immobilized on hydroxyapatite. *RSC Adv.* **2016**, *6*, 78487–78495. [CrossRef]

22. Zou, G.; Zhong, W.; Mao, L.; Xu, Q.; Xiao, J.; Yin, D.; Xiao, Z.; Kirk, S.R.; Shu, T. A non-nitric acid method of adipic acid synthesis: Organic solvent- and promoter-free oxidation of cyclohexanone with oxygen over hollow-structured Mn/TS-1 catalysts. *Green Chem.* **2015**, *17*, 1884–1892. [CrossRef]

23. Tahar, A.; Benadji, S.; Mazari, T.; Dermeche, L.; Marchal-Roch, C.; Rabia, C. Preparation, Characterization and Reactivity of Keggin Type Phosphomolybdates, $H_{3-2x}Ni_xPMo_{12}O_{40}$ and $(NH_4)_{3-2x} Ni_xPMo_{12}O_{40}$, for Adipic Acid Synthesis. *Catal. Lett.* **2015**, *145*, 569–575. [CrossRef]

24. Benadji, S.; Mazari, T.; Dermeche, L.; Salhi, N.; Cadot, E.; Rabia, C. Clean Alternative for Adipic Acid Synthesis Via Liquid-Phase Oxidation of Cyclohexanone and Cyclohexanol Over $H_{3-2x}Co_xPMo_{12}O_{40}$ Catalysts with Hydrogen Peroxide. *Catal. Lett.* **2013**, *143*, 749–755. [CrossRef]

25. Chavan, S.A.; Srinivas, D.; Ratnasamy, P. Oxidation of Cyclohexane, Cyclohexanone, and Cyclohexanol to Adipic Acid by a Non-HNO₃ Route over Co/Mn Cluster Complexes. *J. Catal.* **2002**, *212*, 39–45. [CrossRef]

26. Béziat, J.C.; Besson, M.; Gallezot, P. Liquid phase oxidation of cyclohexanol to adipic acid with molecular oxygen on metal catalysts. *Appl. Catal. A Gen.* **1996**, *135*, L7–L11. [CrossRef]

27. Usui, Y.; Sato, K. A green method of adipic acid synthesis: Organic solvent- and halide-free oxidation of cycloalkanones with 30% hydrogen peroxide. *Green Chem.* **2003**, *5*, 373–375. [CrossRef]

28. Deng, Y.; Ma, Z.; Wang, K.; Chen, J. Clean synthesis of adipic acid by direct oxidation of cyclohexene with H_2O_2 over peroxytungstate-organic complex catalysts. *Green Chem.* **1999**, *1*, 275–276. [CrossRef]

29. Wang, S.-S.; Yang, G.-Y. Recent Advances in Polyoxometalate-Catalyzed Reactions. *Chem. Rev.* **2015**, *115*, 4893–4962. [CrossRef] [PubMed]

30. Zhang, J.; Huang, Y.; Li, G.; Wei, Y. Recent advances in alkoxylation chemistry of polyoxometalates: From synthetic strategies, structural overviews to functional applications. *Coord. Chem. Rev.* **2017**. [CrossRef]

31. Li, T.; Miras, H.; Song, Y.-F. Polyoxometalate (POM)-Layered Double Hydroxides (LDH) Composite Materials: Design and Catalytic Applications. *Catalysts* **2017**, *7*, 260. [CrossRef]

32. Wang, X.; Zhang, X.; He, X.; Ma, A.; Le, L.; Lin, S. Facile Electrodeposition of Flower-Like PMo12-Pt/rGO Composite with Enhanced Electrocatalytic Activity towards Methanol Oxidation. *Catalysts* **2015**, *5*, 1275. [CrossRef]

33. Yu, H.; Ru, S.; Dai, G.; Zhai, Y.; Lin, H.; Han, S.; Wei, Y. An Efficient Iron(III)-Catalyzed Aerobic Oxidation of Aldehydes in Water for the Green Preparation of Carboxylic Acids. *Angew. Chem. Int. Ed.* **2017**, *56*, 3867–3871. [CrossRef] [PubMed]

34. He, P.; Xu, B.; Xu, X.; Song, L.; Wang, X. Surfactant encapsulated palladium-polyoxometalates: Controlled assembly and their application as single-atom catalysts. *Chem. Sci.* **2016**, *7*, 1011–1015. [CrossRef]

35. Al-Oweini, R.; Sartorel, A.; Bassil, B.S.; Natali, M.; Berardi, S.; Scandola, F.; Kortz, U.; Bonchio, M. Photocatalytic Water Oxidation by a Mixed-Valent $Mn^{III}_3Mn^{IV}O_3$ Manganese Oxo Core that Mimics the Natural Oxygen-Evolving Center. *Angew. Chem. Int. Ed.* **2014**, *53*, 11182–11185. [CrossRef] [PubMed]

36. Wu, P.; Yin, P.; Zhang, J.; Hao, J.; Xiao, Z.; Wei, Y. Single-side organically functionalized Anderson-type polyoxometalates. *Eur. J. Chem.* **2011**, *17*, 12002–12005. [CrossRef] [PubMed]

37. Zhang, J.; Huang, Y.; Hao, J.; Wei, Y. β-{Cr[RC(CH$_2$O)$_3$]$_2$Mo$_6$O$_{18}$}$^{3-}$: The first organically-functionalized β isomer of Anderson-type polyoxometalates. *Inorg. Chem. Front.* **2017**, *4*, 1215–1218. [CrossRef]

38. Zhang, J.; Huang, Y.; Zhang, J.; She, S.; Hao, J.; Wei, Y. A direct anchoring of Anderson-type polyoxometalates in aqueous media with tripodal ligands especially containing the carboxyl group. *Dalton Trans.* **2014**, *43*, 2722–2725. [CrossRef] [PubMed]

39. Zhang, J.; Li, Q.; Zeng, M.; Huang, Y.; Zhang, J.; Hao, J.; Wei, Y. The proton-controlled synthesis of unprecedented diol functionalized Anderson-type POMs. *Chem. Commun.* **2016**, *52*, 2378–2381. [CrossRef] [PubMed]

40. Zhang, J.; Liu, Z.; Huang, Y.; Zhang, J.; Hao, J.; Wei, Y. Unprecedented [small chi] isomers of single-side triol-functionalized Anderson polyoxometalates and their proton-controlled isomer transformation. *Chem. Commun.* **2015**, *51*, 9097–9100. [CrossRef] [PubMed]

41. Zhang, J.; Luo, J.; Wang, P.; Ding, B.; Huang, Y.; Zhao, Z.; Zhang, J.; Wei, Y. Step-by-Step Strategy from Achiral Precursors to Polyoxometalates-Based Chiral Organic–Inorganic Hybrids. *Inorg. Chem.* **2015**, *54*, 2551–2559. [CrossRef] [PubMed]

42. Zhang, J.; Zhao, Z.; Zhang, J.; She, S.; Huang, Y.; Wei, Y. Spontaneous resolution of polyoxometalate-based inorganic-organic hybrids driven by solvent and common ion. *Dalton Trans.* **2014**, *43*, 17296–17302. [CrossRef] [PubMed]

43. Alcañiz-Monge, J.; Trautwein, G.; Garcia-Garcia, A. Influence of peroxometallic intermediaries present on polyoxometalates nanoparticles surface on the adipic acid synthesis. *J. Mol. Catal. A Chem.* **2014**, *394*, 211–216. [CrossRef]

44. Nomiya, K.; Takahashi, T.; Shirai, T.; Miwa, M. Anderson-type heteropolyanions of molybdenum(VI) and tungsten(VI). *Polyhedron* **1987**, *6*, 213–218. [CrossRef]

45. Sheldrick, G.M. A short history of SHELX. *Acta Crystallogr. A* **2008**, *64*, 112–122. [CrossRef] [PubMed]

46. Dolomanov, O.V.; Bourhis, L.J.; Gildea, R.J.; Howard, J.A.K.; Puschmann, H. OLEX2: A complete structure solution, refinement and analysis program. *J. Appl. Crystallogr.* **2009**, *42*, 339–341. [CrossRef]

47. Huebschle, C.B.; Sheldrick, G.M.; Dittrich, B. ShelXle: A Qt graphical user interface for SHELXL. *J. Appl. Crystallogr.* **2011**, *44*, 1281–1284. [CrossRef] [PubMed]